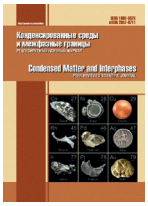

ISSN 1606-867X (Print)
ISSN 2687-0711 (Online)
Condensed Matter and Interphases
Kondensirovannye Sredy i Mezhfaznye Granitsy
https://journals.vsu.ru/kcmf/

Original articles

Research article
https://doi.org/10.17308/kcmf.2022.24/10645

The effect of solution-combustion mode on the structure, morphology and size-sensitive photocatalytic performance of $MgFe_2O_4$ nanopowders

L. A. Lebedev ✉, **M. I. Tenevich, V. I. Popkov**

Ioffe Institute,
26 Politekhnicheskaya str., Saint Petersburg 194021, Russian Federation

Abstract

Ferrites play a significant role in a number of applications from magnetic ceramic to multifunctional catalytic and antimicrobial material. As a catalytic material, it is crucial to have not only high activity but also be made from abounded elements via energy-efficient techniques, to make it valuable for industrial application. Magnesioferrite nanocrystalline powder series were prepared via solution–combustion route while varying fuel/oxidizer ratio. They were investigated by XRD, BET, SEM, DRS, and Fenton-like photocatalytic activity. Temperature-time profiles were measured for the combustion reaction of all mixtures. Results show a strong correlation between fuel content and temperature, structure, and morphology. But de-spite average surface area and crystallite size, the sample synthesized with excess fuel showed high dye adsorption capacity and catalytic activity.

Keywords: Photocatalyst, Ferrites, Spinel, Solution-combustion synthesis, Fenton-like process

Acknowledgments: The XRD and SEM studies were performed on the equipment of the Engineering Center of Saint Petersburg State Institute of Technology.

For citation: Lebedev L. A., Tenevich M. I., Popkov V. I. The Effect of solution-combustion mode on the structure, morphology and size-sensitive photocatalytic performance of $MgFe_2O_4$ nanopowders. *Condensed Matter and Interphases.* 2022;24(4): 496–503. https://doi.org/10.17308/kcmf.2022.24/10645

Для цитирования: Лебедев Л. А., Теневич М. И., Попков В. И. Влияние режима растворного горения на структуру, морфологию и размерно-чувствительные фотокаталитические свойства нанопорошков $MgFe_2O_4$ *Конденсированные среды и межфазные границы.* 2022;24(4): 496–503. https://doi.org/10.17308/kcmf.2022.24/10645

✉ Lev A. Lebedev, e-mail: 1595lion@gmail.com

1. Introduction

In recent years, photocatalytic materials draw significant attention due to their ability to promote a number of chemical processes using a renewable energy source – sunlight. For instance, this type of catalysts can be utilized for several so-called "green processes", from wastewater processing [1–3] and carbon oxide capturing [1–4], to hydrogen production [7] and antibacterial treatment [8, 9]. There are a wide variety of materials that can be used for this purpose, but for commercial applications, materials made from abundant elements are more favourable.

In this research work, magnesium ferrite spinel was the material of choice due to the inexpensiveness of its precursor elements and the known high photocatalytic activity of ferrite spinels [10]. Ferrites are not only catalytically active but also exhibit magnetic properties [11–17], which makes them multifunctional and suitable for facile separation from reaction mass when needed.

Surface properties play a significant role in any heterocatalytic reaction [18]. Therefore, the control over the surface area, its morphology, chemical composition, and some other characteristics, determines the resulting performance of any catalytic material. For the synthetic approach, the solution-combustion technique was selected, because of its short reaction times and energy efficiency [10, 12 19–23].

2. Experimental

2.1. Synthesis

For sample preparation glycine ($C_2H_5NO_2$) was used as fuel and added to an aqueous solution of magnesium ($Mg(NO_3)_2 \cdot 6H_2O$) and ferric ($Fe(NO_3)_3 \cdot 9H_2O$) nitrate in a quartz beaker and heated until water boils off and further to start combustion process (ignition starts at 250-270 °C). All chemicals were used as purchased without further purification. Synthetic ratios were calculated based on equation 1:

$$9Mg(NO_3)_2 + 18Fe(NO_3)_3 + 40C_2H_5NO_2 \rightarrow$$
$$\rightarrow 9MgFe_2O_4 + 100H_2O + 80CO_2 + 56N_2. \quad (1)$$

The stoichiometric factor Φ was proportional to the equation and was equal to 1 for glycine to nitrate ion ratio 5/9, and changed accordingly by multiplication of glycine amount for the same weight of nitrates.

2.2. Characterization

Temperature measurements were conducted using a quartz beaker with inserted K-type thermocouple assembly 0.4 mm in diameter sealed in a glass capillary tube 0.5 mm in diameter attached to ADC-module E20-10 (Lcard) with a sampling rate of 1KSample/s. The miniature size of the thermocouple provides low thermal inertia as well as glass cover prevents short circuits and dissolution by reaction mixture. X-ray diffraction patterns were measured with Rigaku SmartLab3 (Cu-K_α radiation, at I = 50 mA and U = 40 kV). The diffraction patterns of samples were recorded in the Bragg–Brentano focusing geometry with a step of 0.01° and speed of 1°/min in the angle range 10–90°. The specific surface area was measured with Sorbi-M automatic BET sorbtometer. Scanning electron microscopy images were taken with VEGA3 TESCAN scanning electron microscope. Diffusion reflectance and absorption spectra of samples were measured on an Avaspec-ULS2048 compact spectrometer equipped with an AvaSphere-30-Refl integrating sphere for DRS spectra and a 3D-printed cuvette holder for absorption measurements. Catalytic activity was measured via methylene blue discoloration under two 35W Xe-arc lamp irradiation, with 30-minute intervals for two hours total.

3. Results and discussion

3.1. Temperature-time analysis of solution combustion

Temperature-time profiles are shown in Fig. 1a accompanied by a bar graph of the maximum combustion temperature for each sample. It can be noticed that samples with fuel deficiency as well as proficiency have lover reaction temperature compared to the stoichiometric ratio, but the profiles are different. In Fig. 1b, c and d photos of reaction mixtures during each stage of the process are shown, and there is a significant change in the combustion stage. For samples with fuel deficiency combustion followed by the evolution of large amounts of nitrogen oxides that can be observed by the brown coloration of the beaker, it indicates that thermal decomposition

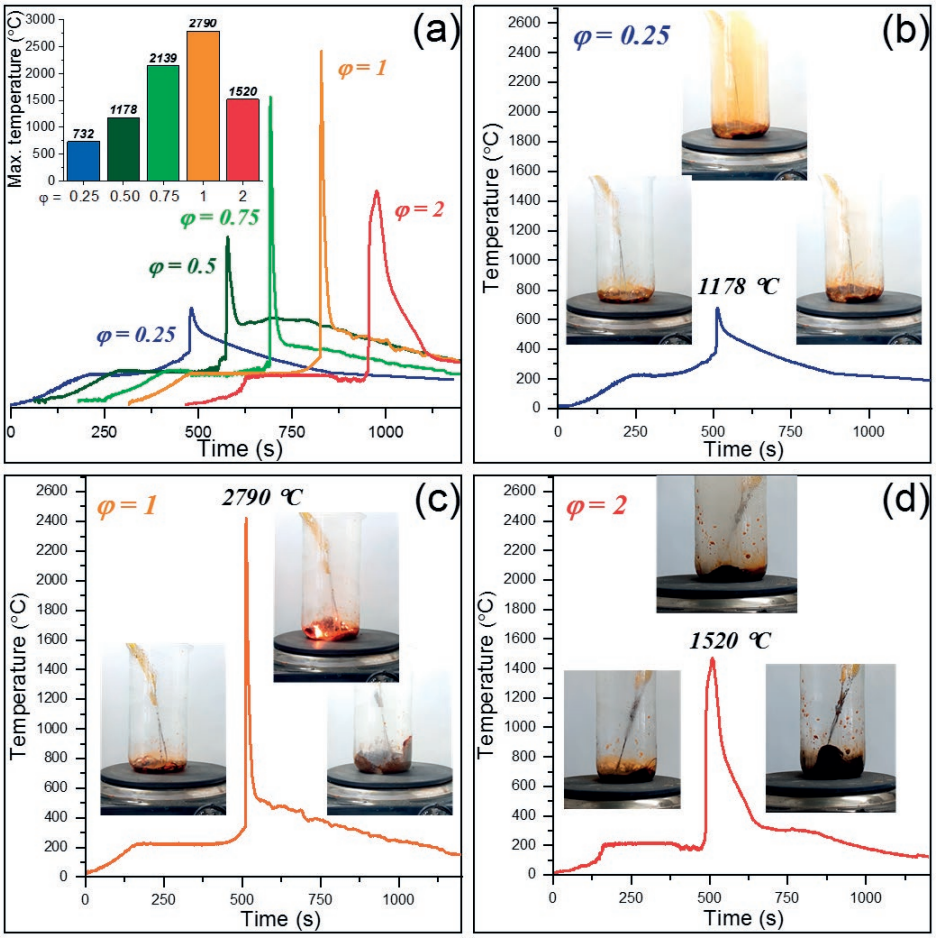

Fig. 1. Time-temperature profiles of solution-combustion synthesis of $MgFe_2O_4$: (a) – comparison of time-temperature profiles of samples with different stoichiometric ratios, insert bar graph shows maximum peak temperature of reaction; (b), (c) and (d) – thermal profiles curves with photos of reaction beaker at different stages of reaction for 0.25, 1 and 2 stoichiometric ratios respectively

of nitrates prevailed for this Φ. That type of combustion mode can be called thermolysis due to prevailing of thermal de-composition over combustion process.

For Φ = 1, combustion proceeds vigorously, with a high amount of energy, seen by a bright glow of reaction products and the absence of fumes, due to most of the products being hot water vapour along with nitrogen and carbon dioxide gases. From the temperature-time profile and visual observation, this combustion mode can be classified as volume type. The maximum temperature was measured as high as 2790 °C while it was in a short period.

Mixture with doubled fuel content (Φ = 2) showed partly similar behavior as fuel deficient mixture, during combustion, large amounts of gases come out along with foaming of products. Thereby, the reaction mixture forms a thermal insulating cocoon, widening the thermal profile peak. The formation of active char foam also prolongs reaction time due to the smoldering process on ambient air. Thus reaction mode can be marked as a smoldering type (24–27).

3.2. X-ray powder diffraction

The structural analysis shown in Fig. 2 confirmed that all prepared samples were magnesioferrite spinels. There is an expected correlation between Φ value and crystallinity, that goes along with maximum temperature change. Higher combustion temperatures provide better crystallinity and bigger crystallite size, where a sample with Φ = 0.25 is al-most amorphous to Φ = 1 with the biggest crystal size and low amorphous phase content.

3.3. The N_2 Adsorption/Desorption Isotherms (BET)

The surface area with SEM photos is presented in Fig. 3. A high correlation of surface area with reaction temperature can be observed, where Φ = 0.25 sample has the highest area, with the lowest reaction temperature, and Φ = 1 sample has the lowest, with the highest combustion temperature, for Φ = 0.5 and 2 area values as well as temperature values are close to each other. From SEM images, fuel deficient sample exhibit a sponge-like structure with big, thin-walled pores that resemble bubbles, stoichiometric sample looks similar to previously mentioned, but most of the "bubbles" are popped and only skeletal borders are left, which could mean that most of the surface gone due to high reaction temperature and melting of thin pore walls. Sample with excess fuel has denser foam-like, compared to previous samples, structure with much smaller pores, but regarding that specific area is not as high as could be expected in comparison with sample Φ = 0.25, which means that some pores are sealed and thus unavailable.

3.4. Diffusion reflectance spectroscopy

Optical band gap values were calculated from diffuse reflective spectra shown in Fig. 4. Fuel ratio-dependent changes in band gap can be observed as a gradual decrease from 2.24 to 2.10 eV with an increase of Φ value, but this change occurs within the 10% region. Nevertheless, this can be utilized to fine-tune material bandgap or make it more susceptible to lower energy irradiation.

3.5. Fenton-like properties

To study the photocatalytic activity of obtained samples, Fenton-like decolorization of methylene blue (MB) dye was used. Absorbance spectra and results of their processing are shown in Fig. 4c-f. From adsorption capacity and photodecomposition rate constant data, one can see that sample with double fuel excess has the most remarkable parameters among some prepared samples, despite the fact of its average specific surface value. Such a significant activity can be attributed to specific surface morphology as well as the number and accessibility of active

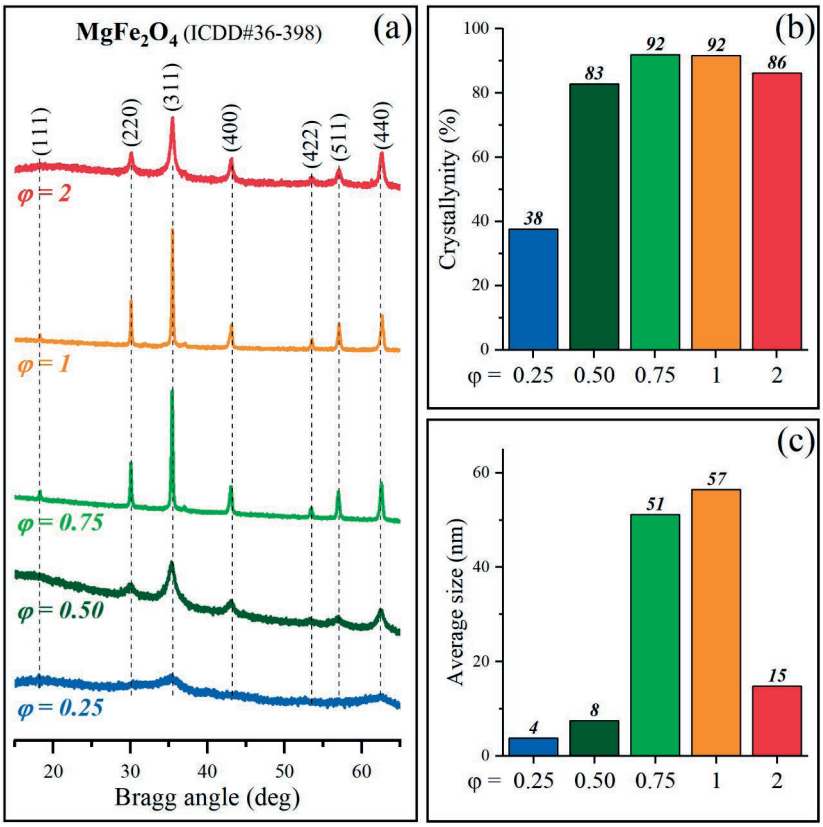

Fig. 2. (a) – XRD patterns of $MgFe_2O_4$ samples; (b) – crystallinity; (c) – average crystal size

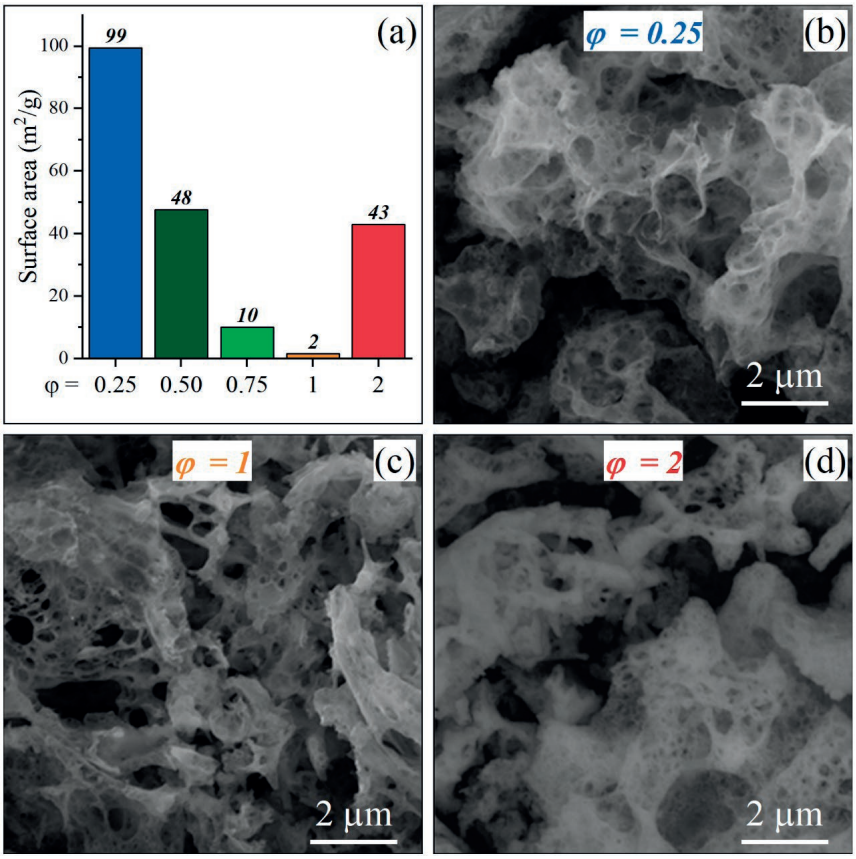

Fig. 3. (a) – BET surface area of spinel samples; (b), (c) and (d) are SEM images of $MgFe_2O_4$ spinels prepared at Φ = 0.25, 1 and 2 respectively

centres. In contrast to samples with Φ in a range from 0.25 to 1, where the main surface species can be oxide or hydroxide groups, because of full combustion and carbon depletion, sample with higher content of the fuel, has a chance to form not only carbon-based structures but also carboxylic, carbonate and other species on the mixed oxide surface, determined by fuel composition and reaction conditions.

4. Conclusions

A highly photo-Fenton-like active $MgFe_2O_4$ spinel sample was synthesized by solution-combustion approach, with variable fuel content Φ. In this research work, it was shown that change in Φ value not only affects combustion temperature but also the combustion mode itself, changing the shape of the temperature-time profile that can result in a combination of morphological, structural, and surface properties. Such a behavior can be observed for half and twice excess of fuel, temperatures are similar and the same for crystallinity and surface area, but due to other types of combustion (smoldering) and thus wider temperature peak, the sample with Φ = 2 has a larger crystallite size, smaller pores, and significantly higher adsorption and catalytic properties. Further investigation of this phenomenon can provide data to additionally enhance the photocatalytic activity of these materials by tuning their properties with reaction conditions such as fuel type and ratio.

Contribution of the authors

The authors contributed equally to this article.

Conflict of interests

The authors declare that they have no known competing financial interests or personal relationships that could have influenced the work reported in this paper.

References

1. Oliveira T. P., Rodrigues S. F., Marques G. N., ... Oliveira, M. M.. $CuFe_2O_4$ for the degradation of dyes

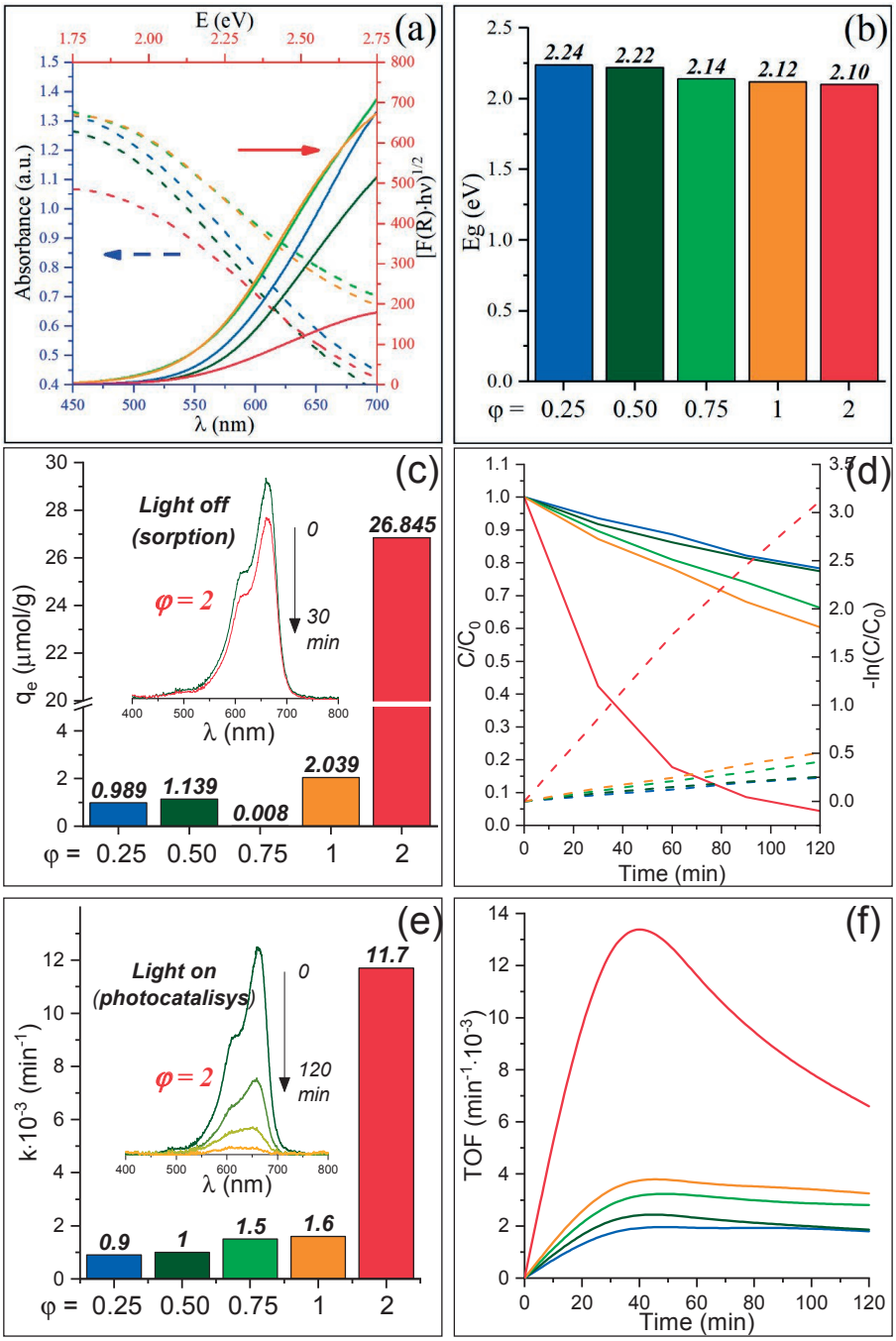

Fig. 4. (a) – dash lines – DRS spectra of samples, solid line – Tauc plots; (b) - optical bandgaps of $MgFe_2O_4$ prepared at different Φ values; (c) – adsorption capacity; insert – absorption spectra of MB solution initial and after 30 minutes of sorption on sample with Φ = 2; (d) - solid line – C/C_0 plot, dash line – $-\ln(C/C_0)$; (e) – photodecomposition rate constant; insert – absorption spectra of MB solution undergoing degradation on sample with Φ = 2 and (f) – turnover frequency of synthesized spinel samples

under visible light. *Catalysts*. 2022;12(6): 623. https://doi.org/10.3390/catal12060623

2. Ali M. A., Idris M. R., Quayum M. E.. Fabrication of ZnO nanoparticles by solution-combustion method for the photocatalytic degradation of organic dye. *Journal of Nanostructure in Chemistry*. 2013;3(1): 2–7. https://doi.org/10.1186/2193-8865-3-36

3. Kefeni K. K., Mamba B. B. Photocatalytic application of spinel ferrite nanoparticles and nanocomposites in wastewater treatment: Review. *Sustainable Materials and Technologies*. 2020;23: e00140. https://doi.org/10.1016/j.susmat.2019.e00140

4. Bowker M. Photocatalytic hydrogen production and oxygenate photoreforming. *Catalysis Letters*.

2012;142(8): 923–929. https://doi.org/10.1007/s10562-012-0875-4

5. Lyulyukin M. N., Kurenkova A. Y., Bukhtiyarov A. V., Kozlova E. A. Carbon dioxide reduction under visible light: a comparison of cadmium sulfide and titania photocatalysts. *Mendeleev Communications*. 2020;30(2): 192–194. https://doi.org/10.1016/j.mencom.2020.03.021

6. Muhammad N. A., Wang Y., Muhammad F. E., He T. Photoreduction of carbon dioxide using strontium zirconate nanoparticles. *Science China Materials*. 2015;58(8): 634–639. https://doi.org/10.1007/s40843-015-0077-7

7. Chandrasekaran S., Bowen C., Zhang P., Li Z., Yuan Q., Ren X. Spinel photocatalysts for environmental remediation, hydrogen generation, CO_2 reduction and photoelectrochemical water splitting. *Journal of Materials Chemistry A*. 2018;6(24): 11078–11104. https://doi.org/10.1039/c8ta03669a

8. Martinson K. D., Beliaeva A. D., Sakhno D. D., ... Popkov V. I. Synthesis, structure, and antimicrobial performance of $Ni_xZn_{1-x}Fe_2O_4$ (x = 0, 0.3, 0.7, 1.0) magnetic powders toward E. coli, B. cereus, S. citreus, and C. tropicalis. *Water*. 2022;14(3): 454. https://doi.org/10.3390/w14030454

9. Maksoud M. I. A. A, El-Sayyad G. S., Ashour A. H., ... El-Okr M. M. Antibacterial, antibiofilm, and photocatalytic activities of metals-substituted spinel cobalt ferrite nanoparticles. *Microbial Pathogenesis*. 2019;127: 144–158. https://doi.org/10.1016/j.micpath.2018.11.045

10. Martinson K. D., Belyak V. E., Sakhno D. D., Kiryanov N. V., Chebanenko M. I., Popkov V. I. Effect of fuel type on solution combustion synthesis and photocatalytic activity of $NiFe_2O_4$ nanopowders. *Nanosystems: Physics, Chemistry, Mathematics*. 2021;12(6): 792–798. https://doi.org/10.17586/2220-8054-2021-12-6-792-798

11. Lomanova N. A., Panchuk V. V., Semenov V. G., Pleshakov I. V., Volkov M. P., Gusarov V. V. Bismuth orthoferrite nanocrystals: magnetic characteristics and size effects. *Ferroelectrics*. 2020;569(1): 240–250. https://doi.org/10.1080/00150193.2020.1822683

12. Lomanova N. A., Tomkovich M. V., Osipov A. V., ... Gusarov V. V. Formation of $Bi_{1-x}Ca_xFeO_{3-\delta}$ nanocrystals via glycine-nitrate combustion. *Russian Journal of General Chemistry*. 2019;89(9): 1843–1850. https://doi.org/10.1134/s1070363219090196

13. Popkov V. I., Almjasheva O. V., Gusarov V. V. Formation mechanism of nanocrystalline yttrium orthoferrite under heat treatment of the coprecipitated hydroxides. *Russian Journal of General Chemistry*. 2015;85(6): 1370–1375. https://doi.org/10.1134/s107036321506002x

14. Kopeychenko E. I., Mittova I. Y., Perov N. S., Nguyen A. T., Mittova V. O., Alekhina Y. A., Salmanov I. V. Nanocrystalline heterogeneous multiferroics based on yttrium ferrite (core) with calcium zirconate (titanate) shell. *Russian Journal of General Chemistry*. 2020;90(6): 1030–1035. https://doi.org/10.1134/s1070363220060158

15. Tomina E. V., Kurkin N. A., Korol' A. K., ... Bui V. X. Spray pyrolysis synthesis, electrical and magnetic properties of $Ho_xBi_{1-x}FeO_3$ nanocrystals. *Journal of Materials Science: Materials in Electronics*. 2022;33(32): 24594–24605. https://doi.org/10.1007/s10854-022-09170-0

16. Vo Q. M., Mittova V. O., Nguyen V. H., Mittova I. Y., Nguyen A. T. Strontium doping as a means of influencing the characteristics of neodymium orthoferrite nanocrystals synthesized by co-precipitation method. *Journal of Materials Science: Materials in Electronics*. 2021;32(22): 26944–26954. https://doi.org/10.1007/s10854-021-07068-x

17. Kopeychenko E. I., Mittova I. Y., Perov N. S., ... Pham V. Synthesis, composition, and magnetic properties of cadmium-doped lanthanum ferrite nanopowders. *Inorganic Materials*. 2021;57(4): 367–371. https://doi.org/10.1134/s0020168521040075

18. Tikhanova S. M., Lebedev L. A., Martinson K. D., ... Popkov V. I. The synthesis of novel heterojunction h-$YbFeO_3$/o-$YbFeO_3$ photocatalyst with enhanced Fenton-like activity under visible-light. *New Journal of Chemistry*. 2021;45(3): 1541–1550. https://doi.org/10.1039/d0nj04895j

19. Abbas R., Martinson K. D., Kiseleva T. Y., Markov G. P., Tyapkin P. Y., Popkov V. I. Effect of fuel type on the solution combustion synthesis, structure, and magnetic properties of YIG nanocrystals. *Materials Today Communications*. 2022;32: 103866. https://doi.org/10.1016/j.mtcomm.2022.103866

20. Martinson K. D., Belyak V. E., Sakhno D. D., Chebanenko M. I., Panteleev I. B. Mn–Zn ferrite nanoparticles by calcining amorphous products of solution combustion synthesis: preparation and magnetic behavior. *International Journal of Self-Propagating High-Temperature Synthesis*. 2022;31(1): 17–23. https://doi.org/10.3103/s106138622201006x

21. Martinson K. D., Belyak V. E., Sakhno D. D., ... Popkov V. I. Solution combustion assisted synthesis of ultra-magnetically soft LiZnTiMn ferrite ceramics. *Journal of Alloys and Compounds*. 2022;894: 162554. https://doi.org/10.1016/j.jallcom.2021.162554

22. Martinson K. D., Sakhno D. D., Belyak V. E., Kondrashkova I. S. $Ni_{0.4}Zn_{0.6}Fe_2O_4$ nanopowders by solution-combustion synthesis: Influence of red/ox ratio on their morphology, structure, and magnetic properties. *International Journal of Self-Propagating High-Temperature Synthesis*. 2020;29(4): 202–207. https://doi.org/10.3103/s106138622004007x

23. Ivanets A. I., Roshchina M. Yu., Prozorovich V. G. Ibuprofen oxidative degradation in the presence of Fenton-catalyst based on $MgFe_2O_4$ nanoparticles.

Proceedings of the National Academy of Sciences of Belarus, Chemical Series. 2019;55(3): 345–351. https://doi.org/10.29235/1561-8331-2019-55-3-345-351

24. Varma A., Mukasyan A. S., Rogachev A. S., Manukyan K. V. Solution combustion synthesis of nanoscale materials. *Chemical Reviews*. 2016;116(23): 14493–14586. https://doi.org/10.1021/acs.chemrev.6b00279

25. Wang X., Qin M., Fang F., Jia B., Wu H., Qu X., Volinsky A. A. Solution combustion synthesis of nanostructured iron oxides with controllable morphology, composition and electrochemical performance. *Ceramics International*. 2018;44(4): 4237–4247. https://doi.org/10.1016/j.ceramint.2017.12.004

26. Siddique F., Gonzalez-Cortes S., Mirzaei A., Xiao T., Rafiq M. A., Zhang X. Solution combustion synthesis: the relevant metrics for producing advanced and nanostructured photocatalysts. *Nanoscale*. 2022;14: 11806–11868. https://doi.org/10.1039/d2nr02714c

27. Ghosh S. K., Prakash A., Datta S., Roy S. K., Basu D. Effect of fuel characteristics on synthesis of calcium hydroxyapatite by solution combustion route. *Bulletin of Materials Science*. 2010;33(1): 7–16. https://doi.org/10.1007/s12034-010-0010-3

Information about the authors

Lev A. Lebedev, Specialist, Junior Research Fellow, Hydrogen Energy Lab, Ioffe Institute, (Saint Petersburg, Russian Federation).

https://orcid.org/0000-0001-9449-9487

1595lion@gmail.com

Maxim I. Tenevich, PhD student, Junior Research Fellow, Hydrogen Energy Lab, Ioffe Institute, (Saint Petersburg, Russian Federation).

https://orcid.org/0000-0003-2003-0672

Vadim I. Popkov, Cand. Sci. (Chem.), Lab Head, Hydrogen Energy Lab, Ioffe Institute, (Saint Petersburg, Russian Federation).

https://orcid.org/0000-0002-8450-4278

vadim.i.popkov@mail.ioffe.ru

Received 01.07.2022; approved after reviewing 18.07.2022; accepted for publication 15.09.2022; published online 25.12.2022.

Translated by the authors